Regional climate model data used within the SWURVE project 1: projected changes in seasonal patterns and estimation of PET

Ekström, M.[1]*, Jones, P.D.[2], Fowler, H.J.[3], Lenderink, G.[4], Buishand, T.A.[5] and Conway, D.[6]

[1, 2] Climatic Research Unit, University of East Anglia, Norwich, UK

[3] Water Resource Systems Research Laboratory, School of Civil Engineering and Geosciences, University of Newcastle, Newcastle upon Tyne, UK

[4, 5] KNMI (Royal Netherlands Meteorological Institute), De Bilt, The Netherlands

[6] School of Development Studies, University of East Anglia, Norwich, UK

* Corresponding author

Dr Marie Ekström
Climatic Research Unit
University of East Anglia
Norwich, Norfolk
NR4 7TJ
United Kingdom

Telephone +44 (0) 1603592721
Fax +44 (0) 1603 507784
Email M.Ekstrom@uea.ac.uk

Abstract

Climate data necessary for studies assessing the risk to various hydrologic and hydraulic systems posed by climate change within SWURVE (Sustainable Water: Uncertainty, Risk and Vulnerability in Europe), was obtained from the regional climate model HadRM3H, developed at the Hadley Centre of the UK Meteorological Office. This paper gives some background to HadRM3H; it also presents anomaly maps of the projected future changes in European temperature, rainfall and potential evapotranspiration (PET, estimated using a variant of the Penman formula).

The future simulations of temperature and rainfall, following the SRES A2 emission scenario, suggest that the majority of Europe will experience future warming in all seasons with heavier precipitation during winter in much of western Europe (with the exception of central and northern parts of the Scandinavian mountains) and drier summers in most parts of western and central Europe (except for the northwest and the eastern part of the Baltic Sea). Particularly large temperature anomalies (> 6 °C) are projected for northeast Europe in winter and for southern Europe and Asia Minor during summer.

The projected PET displayed very large increases during summer for a region stretching from southern France to Russia. The unrealistically large values could be the result of an enhanced hydrological cycle in HadRM3H, affecting several of the input parameters to the PET calculation. To avoid problems with hydrological modelling schemes, PET was re-calculated, this time using an empirical relationship derived from observational values of temperature and PET.

Key words: HadRM3H, temperature, rainfall, PET, Europe

1. Introduction

The most important tools in the study of climate variability and possible future climate change are Coupled Atmosphere-Ocean General Circulation Models (AOGCMs). These models are state-of-the art numerical integrations that represent subsystems of the Earth's climate, and they simulate the large scale state of the global climate. Although AOGCMs are able to reliably simulate the most important large-scale features of the present global climate, they show larger differences in simulated climate, particularly so at finer spatial resolutions, i.e. features, with space scales smaller than a few model grid- boxes (Grotch and MacCracken, 1991; Räisänen, 2000).

There are several reasons for the reduced skill of AOGCMs at the regional or local scale. Firstly, the relatively coarse spatial resolution of the models provides an inadequate description of the structure of the earth's surface; secondly, the hydrodynamics of the atmosphere is non-linear and because of numerical truncation in the models the smallest scales are not resolved; thirdly, sub-grid scale processes in the models, e.g. cloud formation, rainfall, infiltration, evaporation, runoff, are all parameterised, which implies additional uncertainties in the AOGCM simulations (Zorita and von Storch, 1999).

For climate change impact studies with a focus on water management, such as those conducted within the framework of the SWURVE project (Sustainable Water: Uncertainty, Risk and Vulnerability in Europe), a regional to local resolution is essential. The regional detail necessary for hydrological and hydrodynamic studies can be derived from the coarse-scale outputs of global models by simple interpolation, statistical downscaling or high-resolution dynamical modelling, i.e. the use of regional climate models (RCMs) embedded within the global scale AOGCMs. In SWURVE, simulated regional climate data for each of the case study regions were obtained from the RCM, HadRM3H, developed at the Hadley Centre for Climate Prediction and Research at the UK Meteorological Office (Jones et al., 2001b). HadRM3H takes boundary conditions from a coarser resolution global model (see discussion in Hulme et al., 2002), and provides higher spatial resolution (0.44° latitude and 0.44° longitude) of local topography and more realistic simulations of fine-scale weather features for the European area.

Despite their higher spatial resolution, the RCM data are still associated with uncertainty. Although the largest contribution is generally considered to be inherited from the driving AOGCM (Jenkins and Lowe, 2003), the RCM itself is also a source of uncertainty partly due to the limitations in correctly representing sub-grid processes (Hulme et al., 2002). The main sources of uncertainty have been extensively discussed and several recent publications have attempted to account for the influence of uncertainty on model outcomes in general (Wigley and Raper, 2001; Giorgi and Mearns, 2002) and on hydrological applications in particular (Jones, 2000a, b; Anderson et al., 2001; Allen and Ingram, 2002).

In the first part of this two part paper, we examine the general seasonal characteristics of HadRM3H data for two time periods: 1960–1990, representing the present day climate; and the period 2070–2100, representing a future climate influenced by predicted increases in anthropogenic forcings. Three variables, essential to hydrological modelling studies, are discussed; daily surface (1.5 m) temperature, daily rainfall totals (direct outputs from HadRM3H) and potential evapotranspiration (PET), estimated using the FAO (Food and

Agricultural Organization) Penman-Monteith method (Allen et al., 1994). Of particular interest in this paper is the applicability of the FAO PET to the hydrological modelling applications within SWURVE. In the companion paper (Ekström et al., 2004), uncertainty in HadRM3H data is addressed for each of the five European case study regions within SWURVE (see Kilsby et al., 2004).

2. Overview of Hadley Centre's regional modelling scheme

The climate simulations from the Hadley Centre models are realizations of a set of scenarios, which can be thought of as coherent, internally consistent and plausible representations of possible future states of the world (Hulme et al., 2002). The projections of future changes in the climate are based on estimates of future emissions of greenhouse gases and other pollutants, as well as other factors that may influence a future climate. Descriptions of how these atmospheric constituents may change in the future are provided in the Special Report on Emissions Scenarios (SRES) (IPCC, 2000) of the Intergovernmental Panel on Climate Change (IPCC). The report describes a set of storylines that are descriptions of possible future worlds and provide a framework within which future scenarios can be developed.

Four such scenarios were developed for the United Kingdom (UK) by the UK Climate Impacts Programme (UKCIP) (Hulme et al., 2002). The scenarios represent a climate forced by four different levels of emissions: low, medium-low, medium-high and high. The four UKCIP02 scenarios span the IPCC SRES emissions range (i.e. B1–A1F1) and, in terms of probability, are equally plausible representations of future climate.

Physical realizations of the medium-high and the medium-low UKCIP02 scenarios were generated for a European window by the Hadley Centre for Climate Prediction and Research at the UK Met Office using a regional modelling system that comprises three climate models. The different resolution of the models produces a more flexible system that aims to remove some of the large regional circulation errors that generally accompany global coupled models.

The underlying AOGCM, HadCM3 (Gordon et al., 2000), was developed from the earlier coupled model HadCM2 (Johns et al., 1997). Information is exchanged between the ocean and the atmosphere components once a day with heat and water fluxes being conserved exactly (Johns et al., 2003). The atmospheric component of the model (HadAM3) has 19 levels with a spatial resolution of 2.5° latitude by 3.75° longitude (Pope et al., 2000). Compared to HadCM2, HadCM3 includes a new radiation scheme, a new land surface scheme (Cox et al., 1999) and improved representations of penetrative convection, large scale precipitation and cloud schemes (Johns et al., 2003). In addition to the general improvements, the atmospheric component of HadCM3 (HadAM3) also includes a sulphur cycle, which enables it to model transport, chemistry and physical removal processes of anthropogenic sulphate aerosols (Johns et al., 2003). The ocean component of HadCM3 has 20 levels and a higher resolution (1.25° latitude by 1.25° longitude) compared to the atmospheric component, which enables the model to capture important features in the current structure (Wood et al., 1999 in Johns et al., 2003) — for further details on the ocean component see Johns et al. (2003). HadCM3 was initialized, without spinup, from a Levitus observed ocean state with a suitable atmospheric and sea-ice state (see details in Johns et al., 2003). A control integration with fixed forcing provided the climate conditions for the late 19th century. Subsequently a number of experiments with time-varying anthropogenic forcings, including the new IPCC SRES scenarios, were performed (Johns et al., 2003).

The regional detail of the modelling scheme was provided by two other models, HadAM3H and HadRM3H. The first is a global-scale higher resolution (1.25° latitude by 1.875° longitude) version of HadCM3's atmospheric component HadAM3. It was used to give a more accurate representation of the atmospheric response to global sea-surface temperature and sea-ice changes, as simulated by HadCM3 (Jones et al., 2001b). The second model is a regional climate model, which was used to provide the fine-scale spatial detail (0.44° latitude by 0.44° longitude) for an extensive European window (Hulme, et al., 2002). The main benefits of this design are an improved simulation of the strength and position of the North Atlantic storm track and a more realistic representation of clouds and atmospheric humidity, which in turn improve the radiation and precipitation schemes (Jones et al., 2001b).

Due to the large computing costs associated with the regional modelling scheme, the HadAM3H/HadRM3H combination was only run for two time windows: a control period (1960–1990) and a future perturbed run (2070–2100). During the control period HadAM3H was driven with observations of sea-surface temperatures and sea-ice for that period, whilst during the future integration, HadAM3H was driven by changes in SST and sea-ice as simulated by HadCM3, which were added to the observations (Hulme et al., 2002). Observed oceanic data was used instead of modelled due to the relatively poor control climate in HadCM3 (Räisänen et al., 2004).

Three realisations were run for the medium-high scenario (A2 in the SRES) and one for medium-low scenario (B2 in the SRES). Each of the three A2 simulations had identical experimental designs, the same historical changes and the same future changes in greenhouse gases and aerosols, but were initiated from three different points in the control simulation (Hulme et al., 2002). This procedure creates substantial year-to-year and decade-to-decade variability but has little effect on the long-term change (Hulme et al., 2002). Hence the difference between the so called "ensemble" runs relate to the presumed initial conditions in the mid-19th century.

In this paper, the figures illustrating the control simulation and the relative difference of the perturbed period are based on only one ensemble member, A2a. Because long-term changes between the ensemble members are assumed to be similar we would expect little difference compared to the other two ensemble members. Furthermore, the RCMs, which were used to assess uncertainty in the companion paper (Ekström et al., 2004), all used the A2a run to represent the A2 scenario when driven by the HadAM3H. The HadRM3H data were made available via the Climate Impacts LINK project (Viner and Hulme, 1997) website (http://www.cru.uea.ac.uk/link/) at the Climatic Research Unit (CRU) of the University of East Anglia.

3. Estimation of potential evapotranspiration

Whilst daily temperature [°C] and rainfall [mm day^{-1}] are direct outputs from HadRM3H, potential evapotranspiration estimates were calculated for the entire HadRM3H domain using a variant of the Penman-Monteith method; the grass reference evapotranspiration (Eq. 1), developed by the Food and Agricultural Organization (FAO) (Allen et al., 1994). The FAO method defines PET as the potential evapotranspiration from a clipped grass-surface having 0.12 m height and bulk surface resistance equal to 70 s m^{-1} and an assumed surface albedo of 0.23 (Allen et al., 1994). The meteorological variables are assumed to be at a height of 2 m, which is the approximate height of most HadRM3H variables (1.5 m) apart from the wind (10 m). To overcome the height difference for the wind variable, a conversion factor was used to reduce the HadRM3H 10 m wind to the required 2 m height wind (see Allen et al., 1994).

$$PET = \frac{0.408\Delta(R_n - G) + \gamma \dfrac{900}{T + 273.16} U_2 (e_a - e_d)}{\Delta + \gamma(1 + 0.34U_2)}, \qquad (1)$$

where:

PET	:	reference crop evapotranspiration [mm day^{-1}]
R_n	:	net radiation at crop surface [MJ m^{-2} d^{-1}]
G	:	soil heat flux [MJ m^{-2} d^{-1}], here assumed to be 0.
T	:	mean temperature at 2 m height [°C]
U_2	:	wind speed measured at 2 m height [m s^{-1}]
$(e_a$-$e_d)$	:	vapour pressure deficit for measurement at 2 m height [kPa]
Δ	:	slope of the vapour pressure curve [kPa °C^{-1}]

γ : psycrometric constant [kPa °C^{-1}]

900 : coefficient for the reference crop [kJ^{-1} kg K d^{-1}], Allen et al. (1994)

0.34 : wind coefficient for the reference crop [s m^{-1}], Allen et al. (1994)

Wind speed and temperature are direct outputs from HadRM3H. In addition to these, net radiation, vapour pressure deficit and the slope of the vapour pressure curve were calculated using HadRM3H data. More specifically: total cloud, as estimated from long wave radiation from HadRM3H, was used to calculate the relative sunshine fraction; surface temperature (mean, minimum and maximum) and relative humidity were used to calculate the vapour pressure deficit and the slope of the vapour pressure curve, i.e. the change in vapour pressure with temperature.

4. Seasonal anomaly fields

The entire HadRM3H integration domain covers an extensive European window with 111 by 106 grid cells in the latitude/longitude directions (the wind fields are on a staggered grid of 110 by 106 cells). This area includes an 8 grid cell boundary zone (necessary for the nesting within HadAM3H), which has been removed from the maps in this paper.

Seasonal maps of the control period are provided to aid the interpretation of the later anomaly fields (Figures 1, 3, and 5 for temperature, rainfall and PET respectively). The projected changes in temperature, rainfall and FAO PET are shown as seasonal anomalies. The anomalies are created by subtracting the 30-year grid cell averages of the control simulation from the future simulation (Figure 2, 4, and 6 for temperature, rainfall and PET respectively). The seasons were defined as: winter (December to February), spring (March to May), summer (June to August) and autumn (September to November).

The most widespread anomalies in temperature occur during summer (Figure 2c). Average temperature is projected to increase by more than 6 °C for large parts of central/northern Europe, southern Europe and northern Africa. Somewhat larger increases (~7–8 °C) are projected for central-southern France and parts of Russia (~ 60° N and 45° E). More moderate increases (~5–6 °C) are projected for most of central Europe with smaller increases (~2–5 °C) over the British Isles and Fennoscandia. The winter season also shows widespread temperature anomalies (Figure 2a), with a west to east gradient of increasing anomalies from ~3 °C over the British Isles to ~7 °C over central Russia. Two centres with large positive anomalies are evident along the northern rim of the grid; these could be due to a mismatch between the RCM generated dynamics and the forcing boundary fields from the AGCM. During spring (Figure 2b), anomalies typically range from 4 to 7 °C, with even larger increases in northern Russia and northern Finland. Increases tend to be smaller towards the west with the exception of Iberia and large parts of Morocco and Algeria. During autumn, the largest projected increases are in the northern regions of Europe and also Algeria (~ 5°C), with the rest of Europe showing somewhat smaller increases (Figure 2d). In short, temperatures show an increase during all seasons, particularly in southern and central Europe in summer. In other seasons, the greatest increases are found mainly in the northern parts of Russia and northeast Fennoscandia.

The largest projected changes in rainfall occur during winter (Figure 4a) and summer (Figure 4c). During winter, most of Europe with the exception of the central and northern parts of the Scandinavian mountain range, is projected to experience a slight increase in precipitation. The largest increase (>1.5 mm day^{-1}) occurs over the North Sea, southern Norway and over much of the Alps. Projected changes are generally negative during summer, with most of western and central Europe showing a decrease in rainfall that becomes more extreme over the Alps and southern France (<1.5 mm day^{-1}) (Figure 4c). Increases during summer are generally confined to northern Scandinavia and in particular the eastern part of the Baltic Sea. A similar, but less pronounced, pattern to that of summer is also found in autumn (Figure 4d). The other transitional season, spring, is characterized by moderately decreased rainfall over the Iberian Peninsula, parts of Italy and the Balkans (Figure 4b). In short, projected changes to future rainfall have a clear seasonal structure, with the majority of Europe experiencing increases in winter and decreases in summer, and hence a general intensification of today's climate.

For FAO PET (see details in section 3), in all seasons but summer, the PET rate is generally < 5 mm day^{-1} over most of Europe (Figure 5). In summer, however, high rates (~ 10–20 mm day^{-1}) are found across the land areas of the Mediterranean, with even higher rates in southern and central Spain, Turkey and North African countries. The projected change in PET rates for the perturbed climate are shown as anomaly patterns (Figure 6). In summer, very large increases are projected for most of the European landmass with the exception of the British Isles, Scandinavia and northern Russia (Figure 6c). During the other seasons, increases are more moderate. In winter, rates increases by about 1 mm day^{-1} for most of Europe, whilst in spring and autumn, increases are in the range of 1–3 mm day^{-1} (Figure 6b and c for spring and autumn respectively). In both spring and autumn, the increases are larger further south in the HadRM3H window.

5. Validation of FAO PET

The FAO PET for the control simulation was validated against observed PET data for two of the five case study areas: NW England and the Rhine basin. The validation schemes in the respective case study areas were performed, respectively by the partners from University of Newcastle (section 5.1.) and the partners from KNMI (section 5.2.). Both groups discovered what they thought was too a strong temperature dependency in the FAO PET based on the HadRM3H data, giving very high evapotranspiration rates in a future climate. The high rates projected for the future climate were considered unrealistic and not suitable for direct usage in hydrological modelling schemes. Instead of using the FAO PET, both groups decided to use an empirically-derived relationship to estimate PET for their specific case study regions. A summary of the validation exercise and the methodologies used to derive new PET estimations for NW England and the Rhine basin are given below. The potential reasons for the overestimation of PET are discussed in section 6.

5.1. NW England

A direct comparison of the FAO PET based on HadRM3H data and observed data showed an underestimation of the historic annual and monthly PET average for the control simulation. The standard practice for dealing with differences between modelled and observed climate variables has been to apply factors based on the ratio (or sometimes the difference, e.g. for temperature) of the control simulation to observed values on a grid-box basis (as Durman et al., 2001). The daily FAO PET (calculated from HadRM3H) data series were thus 'bias-corrected' by monthly factors (up to 50% increase in summer months) such that the monthly average matched the observed monthly average PET over the 1960–90 period. The future FAO PET time series were adjusted by the same factors.

The use of this approach resulted in much higher daily PET values for daily temperatures over 12 ^{o}C in the control simulation than had occurred historically (not shown). The spread in the FAO PET (HadRMH3) values was also much larger than estimated from observed climatic data. Historic daily values during 1961–1990 were in the range 0.4–3 mm, whereas values of up to 25 mm were predicted for the FAO PET, for essentially the same temperature range. In the future simulation, monthly PET estimates were as high as 370 mm.

Due to the combination of low flows and high temperatures in the case study area during summer, when temperatures are at their highest, it is possible that the unrealistically high FAO PET values could have large effects on the estimation of flow for the future scenarios (Fowler et al., 2004). To avoid this problem a simple regression-based approach was used to recalculate PET for the control and future scenarios. This method assumes that the historic 1961–1990 monthly relationship between temperature and PET (Walsh and Kilsby,

2004) can be extrapolated to a future climate. To compute the new PET values the following approach was used:

1. The coefficients of an empirical Blaney-Criddle equation (Blaney-Criddle, 1950) were derived using historic PET data by Walsh and Kilsby (2004). These were derived using a linear regression of temperature and PET data, (calculated using a Penman-Monteith type formulation) for observed climatic variables in a northwest England catchment in the Lake District region. The equation is given below (see Walsh and Kilsby (2004) for more details):

$$PET_t = p_t(\alpha\ T + \beta)\ , \qquad (2)$$

where PET_t= PET estimated by Penman-Monteith formulation

p_t = mean daily percentage (for the month) of total annual daytime hours

α = empirically derived, 0.456

β = empirically derived, 0.416

T = temperature in °C

2. This formulation equates a linear regression equation for each month between PET and temperature, as the Blaney-Criddle formula is proportional to the Fahrenheit temperature and hence linear in T if T is expressed in degrees Celsius. There was found to be little difference between the historic PET – Temperature relationship for different catchments in NW England and so it is suggested that this relationship may be used successfully for any catchment in NW England.

3. The PET for the control and future simulation of HadRM3H was then computed using the above relationship, but substituting daily temperatures from HadRM3H into the equation to estimate daily PET values.

The differences between monthly mean PET in the future scenario as predicted by the two methods can be seen in Figure 7. The most striking differences occur in summer months, although there are also substantial differences in spring and autumn months. In winter months there is very little difference in future mean monthly PET between the two methods as daily average temperatures rarely reach 12 °C. Figure 8 shows the monthly percentage change in PET predicted for the future simulation (from HadRM3H) by the two methods. The FAO method predicts changes of up to 80% in average monthly PET during August and September and winter increases are predicted to be in the region of 20–30%. The new PET method substantially lowers these estimates of change, with a more uniform change in PET throughout the year. This method predicts increases in PET of between 10 and 20% in all months, with the months from July to September showing slightly larger increases than other months and is used in Fowler et al. (2004).

5.2. The Rhine basin

For the Rhine basin, the FAO PET based on the results of the control simulation of HadRM3H were reasonably close to the PET estimated from observed meteorological data. The observed PET was based on open water evaporation E_o, which was provided by different national Met services. The equations and input data for estimating E_o are therefore not exactly known. For the Swiss part of the basin, however, PET was derived from temperature using the Thornthwaite (1948) formula. After a relatively small bias correction, the mean FAO PET (calculated from HadRm3H) values were very similar to calculations of PET from historical climatic observations. Figure 9 shows a scatter plot of PET against temperature for JJA based on monthly means, averaged over the Rhine area. The spread in the FAO PET computed from HadRM3H data was much larger than the spread in the observed PET. Observed monthly mean values were in the range 2–4 mm day^{-1}, whereas HadRM3H PET values were between 1–9 mm day^{-1}. For the future simulation, the FAO PET during summer increased from 3 mm day^{-1} to nearly 7 mm day^{-1} (after correcting for the small bias in the control climate) and the extreme values increased to nearly 20 mm day^{-1} (not shown).

The large values of bias-corrected FAO PET in dry summer months caused a substantial bias in the mean summer flows (Lenderink et al., 2004). As for the NW England case study (Fowler et al., 2004), an alternative scheme had to be employed to estimate a more realistic future PET. For the Rhine, PET was estimated using a regression of the 10-day mean values of open water evaporation E_o on temperature as follows:

1. A regression was computed for each calendar month and each grid-box. Figure 10 shows a scatter plot of E_o and temperature for a grid-box in the centre of Germany for the month of August. In total 90 points are shown, corresponding to a 30-year period with three 10-day periods in each year. The regression was undertaken with anomalies, so with the mean E_o and temperature (over these 90 points) subtracted. The regression coefficient (the slope of the fit) is denoted α_{local}.

2. The regression coefficients were averaged over the Rhine basin, giving α_{area}. This spatial averaging was performed to filter out noise.

3. Due to the spatial averaging all spatial information is lost. This leads to problems over mountainous areas where the mean values of E_o are low, causing negative values of the re-computed E_o when the relatively large area mean α_{area} is used. Therefore, a local correction was applied based on the local 30-year average open water evaporation $\overline{E}_{\mathrm{o,local}}$ for the month of interest divided by the 30-year area-average open water evaporation $\overline{E}_{\mathrm{o,area}}$ for that month.

4. The evaporation anomaly $\Delta E_o(t)$, with respect to the local mean for the month of interest, is computed from

$$\Delta E_{\mathrm{o}}(t) = \alpha_{\mathrm{area}} \frac{\overline{E}_{\mathrm{o,local}}}{\overline{E}_{\mathrm{o,area}}} \Delta T(t), \quad t = 1, \ldots, 36J \tag{3}$$

   with $\Delta T(t)$ the temperature anomaly (again compared to the local mean for the month of interest), and J the number of years.

The values from the Thornthwaite formula for Swiss part of the basin could not be used for the estimation of the spatial average relationship in step 2. They were, however, included in the area-averages $\overline{E}_{\mathrm{o,area}}$.

The relative domain-averaged changes in E_o per degree (basin mean change divided by the basin mean E_o) are shown in Figure 11. For the summer, the increase in E_o is nearly 8% per degree temperature change (to compare with an increase of about 4% in PET per degree temperature change for the method described in section 5.1).

The relatively large increase in E_o from a regression of E_o on temperature for the present climate may lead to an overestimation of evaporation in the future climate (Brandsma, 1995). Fortunately, with a simple manipulation of the temperature anomalies of the future climate run, it is possible to obtain different scenarios for E_o from Eq. (3). These temperature anomalies can be split into a contribution of the mean temperature change between future and control climate, $\overline{T}_{\mathrm{fut}} - \overline{T}_{\mathrm{cont}}$ (as a function of time of the year and location), and a remaining part accounting for variations in the weather:

$$\Delta T_{\mathrm{fut}}(t) = T_{\mathrm{fut}}(t) - \overline{T}_{\mathrm{cont}} = \left[\overline{T}_{\mathrm{fut}} - \overline{T}_{\mathrm{cont}}\right] + \left[T_{\mathrm{fut}}(t) - \overline{T}_{\mathrm{fut}}\right], \quad t = 1, \ldots, 36J \qquad (4)$$

where $T_{\mathrm{fut}}(t)$ are the simulated 10-day temperatures for the future climate.

Three different scenarios for the future E_o were constructed by multiplying the mean temperature-change related contribution by a factor β:

- β = 0.0 (low scenario). This scenario represents a lower limit giving no change in the mean E_o.

- β = 0.5 (middle scenario), giving an increase of about 25% in E_o in summer, or nearly 4% per °C, which is very similar to the increase found in section 5.1 and to the increase in the scenarios used by Shabalova et al. (2003) in an earlier application of regional climate model output to the Rhine basin.

- β =1.0 (high scenario), representing an extrapolation of the present E_o temperature relation to the future climate.

Crop factors were then used to convert the E_o values to potential evaporation.

6. Discussion and conclusions

The future simulations of HadRM3H temperature and rainfall, following the A2 emission scenario, suggest that the majority of Europe will experience future warming in all seasons, (Figure 2), with heavier precipitation during winter in much of western Europe (with the exception of central and northern parts of the Scandinavian mountains) (Figure 4a) and drier summers in most parts of western and central Europe (except for the northwest and the eastern part of the Baltic Sea) (Figure 4d). Particularly large temperature anomalies (> 6 °C) are projected for northeast Europe in winter (Figure 2a) and for southern Europe and Asia Minor during summer (Figure 2c).

The simulation of summer temperature in south-eastern Europe and Asia Minor is however known to be associated with a warm bias, seen not only in HadRM3H (Jones et al., 2001b) but also in many other RCMs (Hagemann et al., 2001). Jones et al. (2001b) describe this problem in some detail. An unfortunate side effect of increasing the resolution in HadAM3H is the worsening of an already existing warm bias in the summer temperatures over large parts of Europe, with the increased resolution upsetting a balance of errors operating in HadAM3, the atmospheric component of HadCM3 (Jones et al., 2001b). More specifically, the increased resolution leads to an intensification of the hydrological cycle (stronger surface winds and evaporation, stronger vertical motion, reductions in atmospheric relative humidity and more heavy precipitation events) (Jones et al., 2001b). The intensified hydrological cycle, however, also leads to lower cloud cover, which is already low in HadAM3 but to some degree balanced by other biases. With lower cloud cover follows increased insolation, which results in increased surface heating. To counteract the problem some modifications were made to the cloud physics in the model and the coupling between the soil and the land surface in HadAM3H in order to improve on the simulation of the summer temperature whilst keeping the high resolution (Jones et al., 2001b). Comparison with HadAM3 showed that the modifications reduced the warm bias in large parts of Europe. However, the bias still remains in southeast Europe and Asia Minor (Jones et al., 2001b). It is not clear therefore, whether the large warming in southeast Europe and Asia Minor in summer can be considered as ‘real’ or enhanced by limitations in representing the hydrodynamics by the RCM.

Of particular interest in this paper was the estimation of PET, which is necessary for hydrological modelling in the case study regions. It should be noted that HadRM3H does not give PET, as it calculates the actual evapotranspiration directly. This paper showed how outputs from HadRM3H could be used in combination with a variant of the Penman-Monteith method developed by the FAO (Allen et al., 1994) (Eq. 1), to estimate PET for the

HadRM3H window. However, comparisons of the control simulation FAO PET and observed data for the NW England and the Rhine basin showed that the FAO PET values were larger compared to the observational estimates. Furthermore, the future FAO PET values were clearly not physically realistic and should therefore not be used for hydrological simulations in these regions. Instead, PET was estimated directly from temperature using empirical relationships based on observed meteorological data from each specific location.

Given that the FAO method has previously been selected above several other methods in a comparative test to estimate PET for European environments (Jones et al., 2001a), it was surprising to find such poor results, primarily during summertime, using the HadRM3H data. The intensification of the hydrological cycle due to the use of higher resolution in the regional modelling scheme, as described by Jones et al. (2001b), could however be the underlying cause for these extreme PET values. An unrealistically large hydrological feedback in HadRM3H generated climate would cause dry conditions leading to low cloud amounts, high surface radiation, high surface temperatures and consequently high vapour pressure deficits near the surface. If this was the case, large changes in these variables would be expected between the control and the future simulation. Therefore, anomaly maps of the future compared to the control simulation were created for those variables that were expected to have the largest influence on the magnitude of the FAO PET: relative humidity [%], temperature [°C], total cloud from long wave radiation [fraction] (all three are HadRM3H variables) and vapour pressure deficit [kPa] (the difference between the saturation vapour pressure and the actual vapour pressure, calculated in the FAO method) (Figure 12c). The graphs were prepared using only one of the three HadRM3H ensemble members (A2a), as the same trend would be expected in all HadRM3H model experiments. Furthermore, only summer data were used as the impact of the hydrological feedback should be largest during the warm season.

The maps showed that most regions with large predicted increases in summer temperatures (Figure 12a) also showed large decreases (-10 to -40 %) in predicted relative humidity by HadRM3H (Figure 12b), which in combination with the high temperatures produced large increases in the vapour pressure deficit (Figure 12c). A region stretching from southern France, crossing central Europe and stretching to Russia was predicted to have an overall increase in vapour pressure deficit of around 0.1 to 0.2 kPa (or 100 %) (Figure 12c). Even larger increases were predicted in some isolated areas of France, the Netherlands, Germany and Russia. This increase is directly linked to the increased drying power of the air. In addition to the changes in vapour pressure, PET was further enhanced by increases in the net radiation term. The reduced cloud coverage in the future climate (Figure 12d) leads to an increase in the net shortwave radiation term and hence an overall increase in the total net radiation term. Considering all maps, however, the similarity in the spatial patterns and magnitude of change between the PET (Figure 6c) and vapour pressure deficit (Figure 12c) clearly indicated that the latter was the main cause of the high evapotranspiration rates when using the FAO method in combination with direct output of HadRM3H. Furthermore, it is probable that the high vapour pressure deficits in HadRM3H are related to the lack of sufficient low to middle level clouds in the regional modelling scheme (pers. comm. Richard Jones). A relationship between cloud cover and PET has been shown in observed data by Roderick and Farquhar (2002), who found reductions of pan evaporation during the warmer latter half of the 20th Century, which they related to increased cloud coverage and aerosol concentration.

It is clear that there are aspects of the hydrological cycle that can be further improved in climate models. In addition to cloud parameterizations, which have been subject to large improvements in different generations of Hadley Centre models, there is also room for improvement in describing the interactions between the atmosphere and the land surface. There are recent publications that address this issue using observed data (Koster et al., 2003; Pal and Eltahir, 2002). In Koster et al. (2003) it was suggested that although the evidence for land-atmosphere feedback was not conclusive, results showed an agreement between structures in precipitation variance and autocorrelation fields between a 50-year observational precipitation data set and those produced by an AGCM. Furthermore, Pal and Eltahir (2002) showed that depending on the location, soil moisture anomalies over relatively small regions could significantly alter rainfall both locally and in surrounding regions in North America.

For SWURVE, the unrealistically high FAO PET values justify the modifications to the PET by the SWURVE partners. There are wider ramifications, however, which mean that RCM output should only be used with caution when used directly in a downstream impact model (e.g. the rainfall/runoff models used by SWURVE partners). A sensible exercise would be to first assess the RCM's reliability against observational data and consider the realism of projected change in the perturbed run that simulates the future. However, some modifications that could improve the hydrological cycle in the regional modelling scheme have been included by the Hadley Centre in their new version of the RCM, HadRM3P (Richard Jones, pers. com., in Moberg and Jones, 2004). Differences between HadRM3P and HadRM3H are however, very small for temperature and precipitation and this suggests that potential PET biases would still be large if a Penman type formula were to be used. Bias would likely be smaller if simpler PET formulae (such as Thornthwaite (1948) or Blaney Criddle (1950)), which assume only temperature dependence, were used.

6. Acknowledgments

We would like to thank David Viner Climatic Research Unit, University of East Anglia, UK) for aiding the access to HadRM3H data, which were supplied by the Climate Impacts LINK project (DEFRA Contract EPG 1/1/154) on behalf of the Hadley Centre and U.K. Meteorological Office. The meteorological data for the Rhine basin were made available by the following institutions: Deutscher Wetterdienst, Service de la météorologie et de l'hydrologie de Luxembourg, Météo France and Swiss Meteorological Institute, via the International Commission for the Hydrology of the Rhine basin (CHR/KHR). This work is part of the SWURVE (Sustainable Water: Uncertainty, Risk and Vulnerability Estimation in Europe) project, partly funded under the EU Environment and Sustainable Development programme, grant number EVK1-2000-00075.

References

Allen, M.R. and Ingram, W.J., 2002. Constraints on future changes in climate and the hydrologic cycle, Nature, 419, 224-232.

Allen, R.G., Smith, M., Pereira, L.S. and Perrier, A., 1994. An update for the calculation of reference evapotranspiration. ICID Bulletin, 43, 35-92.

Anderson, M.L., Kavvas, M.L. and Mierzwa, M.D., 2001. Probabilistic/ensemble forecasting: a case study using hydrologic response distributions associated with El Nino/Southern Oscillation (ENSO), J. Hydrol., 249, 134-147.

Blaney, H.F. and Criddle, W.D., 1950. Determining water requirements in irrigated areas from climatological and irrigation data, USDA, Soil Conservation Service, TP-96.

Brandsma, T., 1995. Hydrological impact of climate change, a sensitivity study for the Netherlands. PhD thesis, Delft University of Technology.

Cox, P., Betts, R.A., Bunton, C., Essery, R., Rowntree, P.R.R. and Smith, J., 1999. The impact of new land surface physics on the GCM simulation of climate and climate sensitivity, Clim. Dyn., 15,183-203.

Durman, C.F., Gregory, J.M., Hassell, D.C., Jones, R.G., and Murphy, J.M., 2001. A comparison of extreme European daily precipitation simulated by a global and a regional climate model for present and future climates, Q. J. Roy. Meteorol. Soc., 127, 1005-1015.

Ekström, M., Hingray, B., Mezghani, A. and Jones, P.D., 2004. Regional climate model data used within the SWURVE project 2: addressing uncertainty in regional climate model data for five European case study areas, Hydrol. Earth Syst. Sci.

Fowler, H.J., Kilsby, C.G. and Stunell, J. 2004. Modelling the impacts of projected future climate change on water resources in northwest England, Hydrol. Earth Syst. Sci.

Giorgi, F. and Mearns, L.O., 2002. Calculation of Average, Uncertainty Range, and Reliability of Regional Climate Changes from AOGCM Simulations via the “Reliability Ensemble Averaging” (REA) method, J. Clim., 1141-1158.

Gordon, C., Cooper, C., Senior, C.A, Banks, H.T., Gregory, J.M., Johns, T.C., Mitchell, J.F.B., Wood, R.A., 2000. The simulation of SST, sea ice extents and ocean heat transports in a version of the Hadley Centre coupled model without flux adjustments. Clim. Dyn., 16, 147-168.

Grotch, S.L. and MacCracken, M.C., 1991. The use of general circulation models to predict regional climate change, J. Clim., 4, 286-303.

Hagemann, S., Botzet, M. and Machenhauer, B., 2001. The Summer Drying Problem Over South-Eastern Europe: Sensitivity of the Limited Area Model HIRHAM4 to Improvements in Physical Parameterization and resolution. Phys. Chem. Earth (B), 26, 391-396.

Hulme, M., Jenkins, G.J., Lu, X., Turnpenny, J.R., Mitchell, T.D., Jones, R.G., Lowe, J., Murphy, J.M., Hassell, D., Boorman, P., McDonald, R. and Hill, S., 2002. Climate Change Scenarios for the United Kingdom: The UKCIP02 Scientific Report, Tyndall Centre for Climate Change Research, School of Environmental Sciences, University of East Anglia, Norwich, UK, 112 pp.

IPCC, 2000. Technical Summary. In: Nakicenovic, N. and Swart, B (Eds). Special Report on Emissions Scenarios. Cambridge Univ. Press, Cambridge.

Jenkins, G. and Lowe, J., 2003. Handling uncertainties in the UKCIP02 scenarios of climate change. Hadley Centre Technical note 44.

Johns, T.C., Carnell, R.E., Crossley, J.F., Gregory, J.M., Mitchell, J.F.B., Senior, C.A., Tett, S.F.B. and Wood, R.A., 1997. The second Hadley Centre Coupled Ocean-Atmosphere GCM: Model Description, Spinup, and Validation. Clim. Dyn., 13,103-134.

Johns, T.C., Gregory, J.M. Ingram, W.J., Johnson, C.E., Jones, A., Lowe, J.A., Mitchell, J.F.B., Roberts, D.L., Sexton, D.M.H., Stevenson, D.S., Tett, S.F.B. and Woodage, M.J., 2003. Anthropogenic climate change for 1860 to 2100 simulated with the HadCM3 model under updated emissions scenario, Clim. Dyn., 20, 583-612.

Jones, R.N., 2000a. Analysing the risk of climate change using an irrigation demand model, Clim. Res., 14, 89-100.

Jones, R.N., 2000b. Managing uncertainty in climate change projections - issues for impact assessments, Climate Change, 45, 403-419.

Jones, P.D., Reid, P. and Conway, D., 2001a. Data sets and scenarios. In: Kilsby, C. (Ed): Water Resources: Influence of Climate change in Europe. Final Report WRINCLE, EU Environment and Climate Research Programme ENV4-CT97-0452, Univ. of Newcastle, Newcastle, 4-18.

Jones, R., Murphy, J., Hassell, D. and Taylor, R., 2001b. Ensemble mean changes in a simulation of the European climate of 2071-2100 using the new Hadley Centre regional modelling system HadAM3H/HadRM3H. Hadley Centre, Met. Office Bracknell, UK.

Kilsby, C., 2004. Sustainable Water: Uncertainty Risk and Vulnerability in Europe. Hydrol. Earth Syst. Sci. (this issue)

Koster, R.D., Suarez, M.J., Higgins, R.W. and Van den Dool, H.M., 2003. Observational evidence that soil moisture variations affect precipitation, Geophysical Research Letters, 30, 1241,doi:10.1029/2002GL016571

Lenderink, G., Buishand, T.A. and van Deursen, W.P.A., 2004. Estimates of future discharges of the river Rhine using two climate scenario methodologies: direct versus delta approach, Hydrol. Earth Syst. Sci.

Moberg, A. and Jones, P.D., 2004. Regional Climate Model simulations of daily maximum and minimum near-surface temperatures across Europe compare with observed station data 1961-1990. Clim. Dyn. Submitted

Pal, J.S. and Eltahir, E.A.B., 2002. Teleconnections of soil moisture and rainfall during the 1993 midwest summer flood, Geophys. Res. Lett., 29, 1865, doi:10.1029/2002GL014815.

Pope, V.D., Gallani, M.L., Rowntree, P.R. and Stratton, R.A., 2000. The impact of new physical parameterizations in the Hadley Centre climate model: HadAM3, Clim. Dyn., 16, 123-146.

Roderick, M.L. and Farquhar, G.D., 2002. The Cause of Decreased Pan Evaporation over the Past 50 Years, Science, 298, 1410-1411.

Räisänen, J., 2000. CO_2-induced climate change in northern Europe: comparison of 12 CMIP2 experiments, SMHI Reports Meteorology Climatology 87.

Räisänen, J., Hansson, U., Ullerstig, A., Döscher, R., Graham, L.P., Jones, C., Meier, M., Samuelsson, P. and Willén, U., 2004. European climate in the late twenty-first century: regional simulations with two driving global models and two forcing scenarios. Clim. Dyn.,22, 13-31.

Shabalova, M.V., van Deursen, W.P.A. and Buishand, T.A., 2003. Assessing future discharge of the river Rhine using regional climate model integrations and a hydrological model, Clim. Res., 23, 233-246.

Thornthwait, C.W., 1948. An approach towards a rational classification of climate, Geog. Rev., 38, 55-94.

Viner, D. and Hulme, M., 1997. The Climate Impacts LINK Project: Results of the Hadley Centre's Climate Change Experiments for Climate Change Impacts Assessments. UK DETR Report, Climatic Research Unit, University of East Anglia, Norwich, UK.

Walsh, C. and Kilsby, C., 2004. Salmon physical habitat under changed climates. Hydrol. Earth Syst. Sci. (this issue)

Wigley, T.M.L. and Raper, S.C.B., 2001. Interpretation of high projections for global-mean warming, Science, 293, 451-454.

Wood, R.A., Keen, A.B., Mitchell, J.F.B. and Gregory, J.M., 1999. Changing spatial structure of the thermohaline circulation in response to atmospheric CO_2 forcing in a climate model, Nature, 399, 572-575.

Zorita, E. and von Storch, H., 1999. The analog method as a simple statistical downscaling technique: Comparison with more complicated methods, J. Clim.,12, 2474-2489.

Figure texts

Figure 1. Seasonal averages of temperature [°C at 1.5 m] for the entire HadRM3H integration domain for the period 1960–1990; a) winter (December to February), b) spring (March to May), c) summer (June to August) and d) autumn (September to November).

Figure 2. Seasonal temperature anomalies [°C at 1.5 m] for the entire HadRM3H integration domain (difference between the periods 2070–2100 and 1960–1990): a) winter (December to February), b) spring (March to May), c) summer (June to August) and d) autumn (September to November).

Figure 3. Seasonal averages of rainfall [mm day^{-1}] for the entire HadRM3H integration domain for the period 1960–1990; a) winter (December to February), b) spring (March to May), c) summer (June to August) and d) autumn (September to November).

Figure 4. Seasonal rainfall anomalies [mm day^{-1}] for the entire HadRM3H integration domain (difference between the periods 2070–2100 and 1960–1990): a) winter (December to February), b) spring (March to May), c) summer (June to August) and d) autumn (September to November).

Figure 5. Seasonal averages of FAO potential evapotranspiration [mm day^{-1}] for the entire HadRM3H integration domain for the period 1960–1990; a) winter (December to February), b) spring (March to May), c) summer (June to August) and d) autumn (September to November).

Figure 6. Seasonal FAO potential evapotranspiration anomalies [mm day^{-1}] for the entire HadRM3H integration domain (difference between the periods 2070–2100 and

1960–1990): a) winter (December to February), b) spring (March to May), c) summer (June to August) and d) autumn (September to November).

Figure 7. Mean monthly PET for historic observations (1961–1990), control and future scenarios for the NW England case study area. Blaney-Criddle indicates scenarios where the observed relationship between PET and temperature has been used to construct PET series. Penman BC indicates scenarios where the FAO Penman-Monteith equation has been used to construct PET series with bias correction (BC). Note that "Historic,1961-1990" and "Control Blaney-Criddle" are very similar, hence the former obscure the latter in the figure.

Figure 8. Percentage monthly increases in PET for the period 2070–2100 in the NW England case study area compared to the period 1961–1990, predicted by the FAO Penman-Monteith equation with bias correction (Future Penman BC) and the PET estimated from the observed Blaney-Criddle relationship between PET and temperature (Future Blaney-Criddle).

Figure 9. Scatter plot of (basin-average) PET [mm day-1] against temperature [°C] for each month in summer (June to August). Results are shown for the observations (circles) and HadRM3H data (dots).

Figure 10. Scatter plot of PET [mm day-1] against temperature [°C] for each 10-day period in August for one location in the centre of Germany.

Figure 11. The domain-averaged relative change in E_o per degree (basin-average change divided by basin-average E_o) obtained with both methods.

Figure 12. Summer anomalies between HadRM3H control and future simulation (following the A2 emissions scenario) for a) temperature [°C], b) relative humidity [%], c) vapour pressure deficit [kPa] and d) total cloud [Fraction].

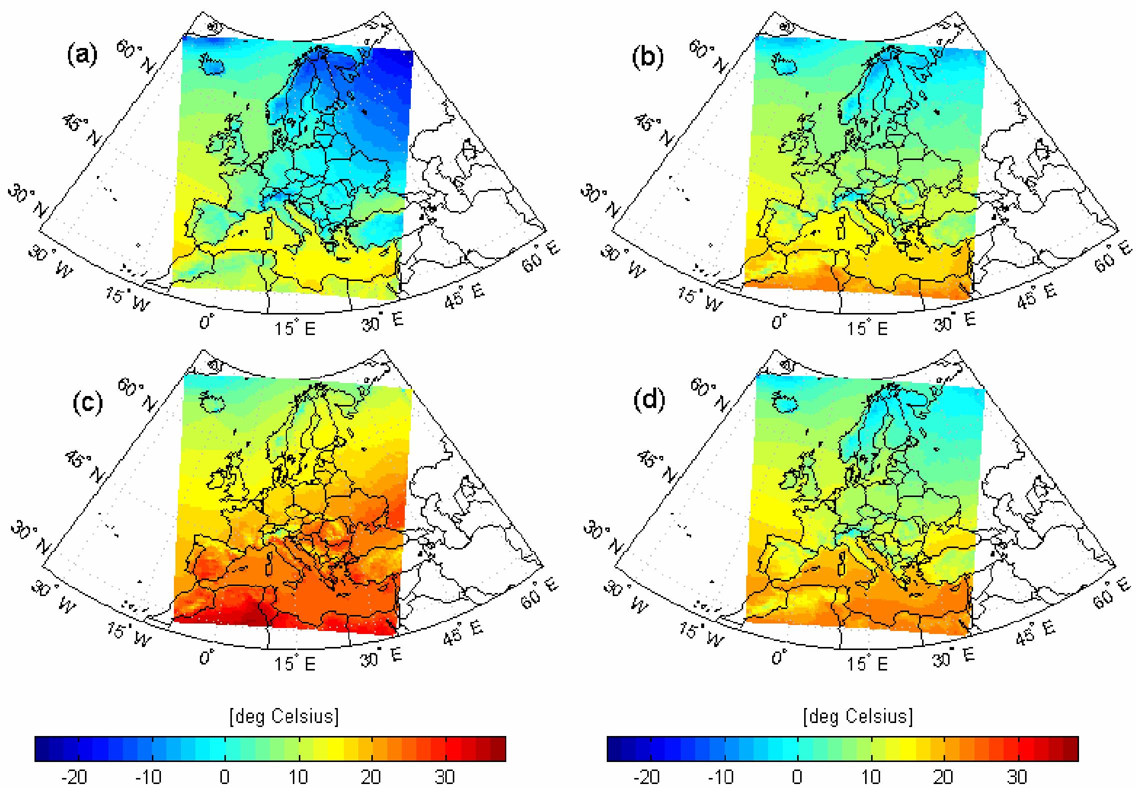
(a)
(b)
(c)
(d)
60° N
45° N
30° N
30° W
15° W
0°
15° E
30° E
45° E
60° E
[deg Celsius]
-20
-10
0
10
20
30

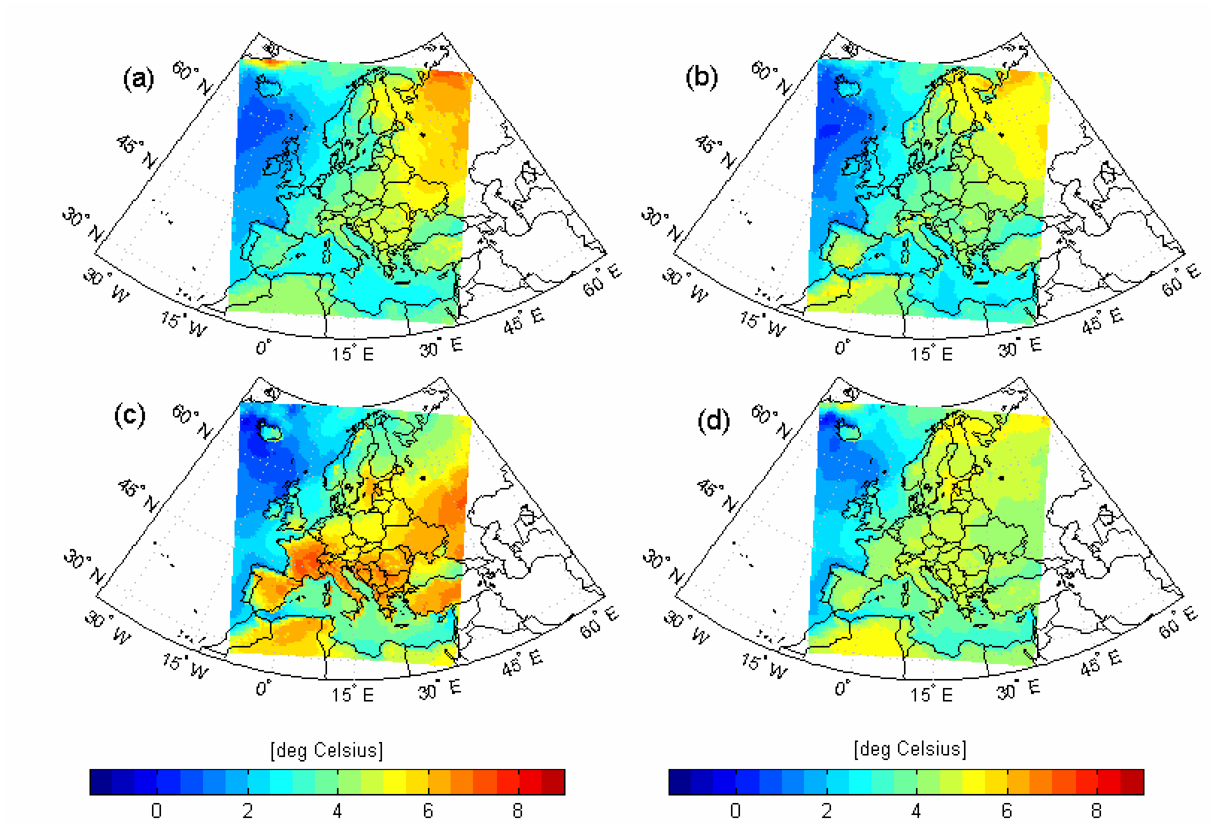

(a)
(b)
(c)
(d)
60° N
45° N
30° N
30° W
15° W
0°
15° E
30° E
45° E
60° E
[deg Celsius]
0
2
4
6
8

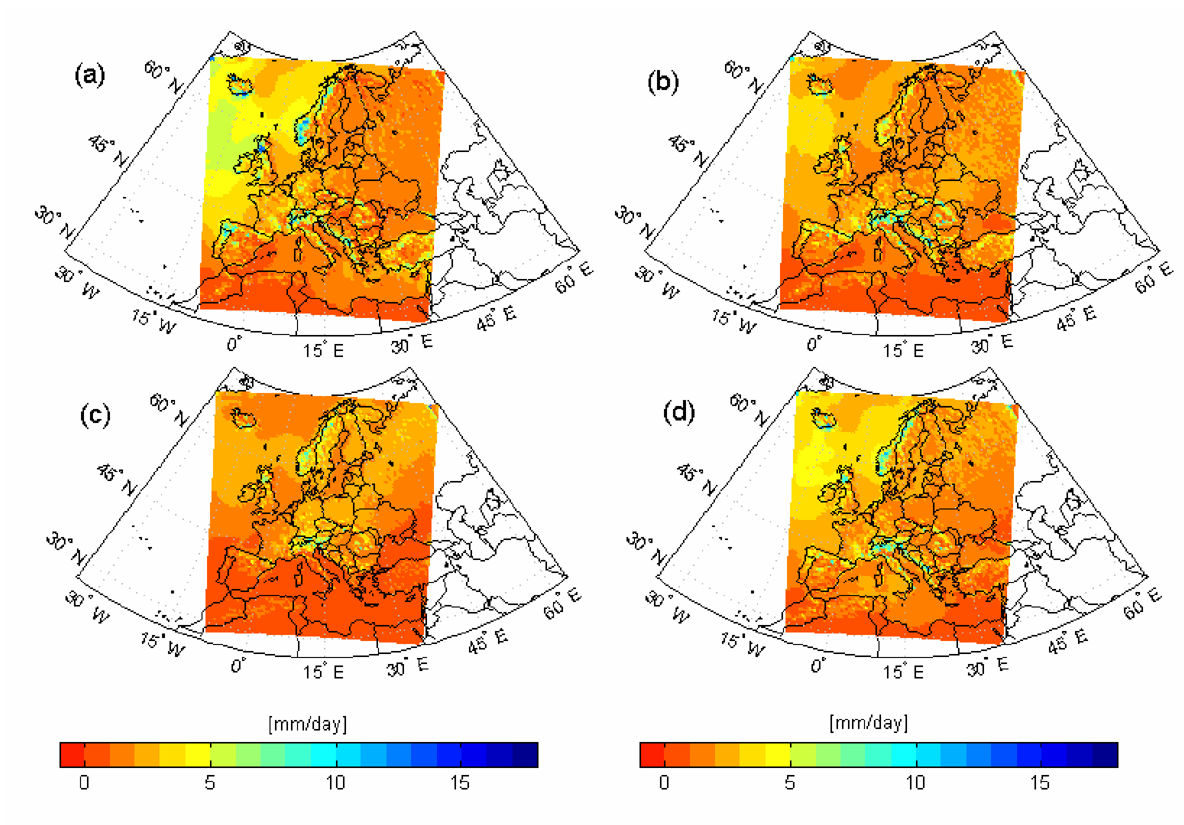
(a)
(b)
(c)
(d)
60° N
45° N
30° N
30° W
15° W
0°
15° E
30° E
45° E
60° E
[mm/day]
0
5
10
15

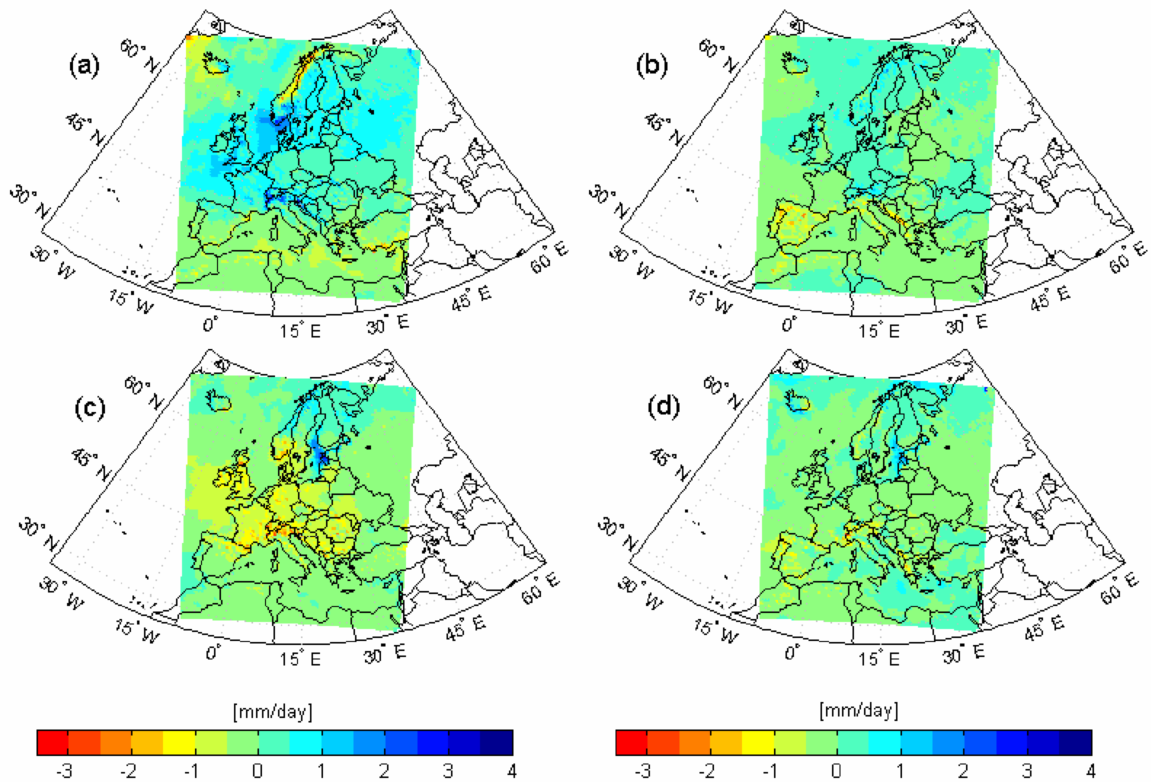
(a)
(b)
(c)
(d)
60° N
45° N
30° N
30° W
15° W
0°
15° E
30° E
45° E
60° E
[mm/day]
-3
-2
-1
0
1
2
3
4

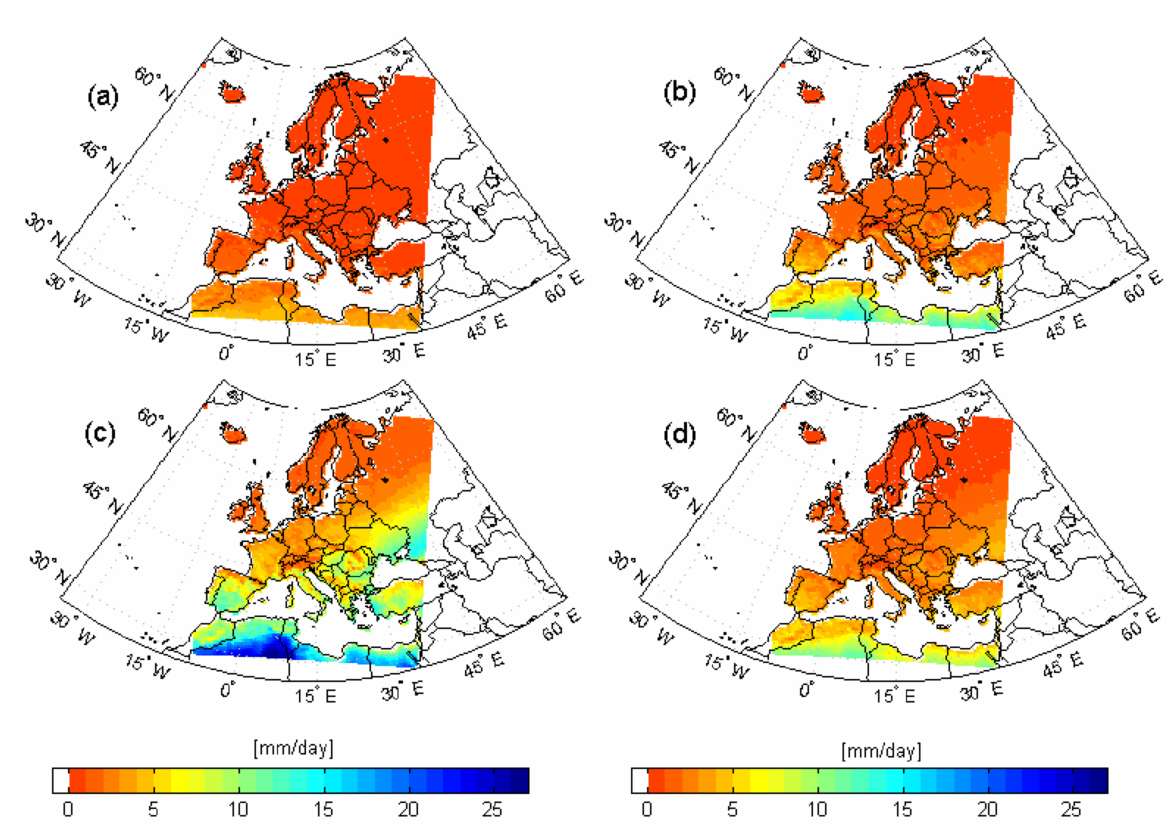

(a)
(b)
(c)
(d)
60° N
45° N
30° N
30° W
15° W
0°
15° E
30° E
45° E
60° E
[mm/day]
0
5
10
15
20
25

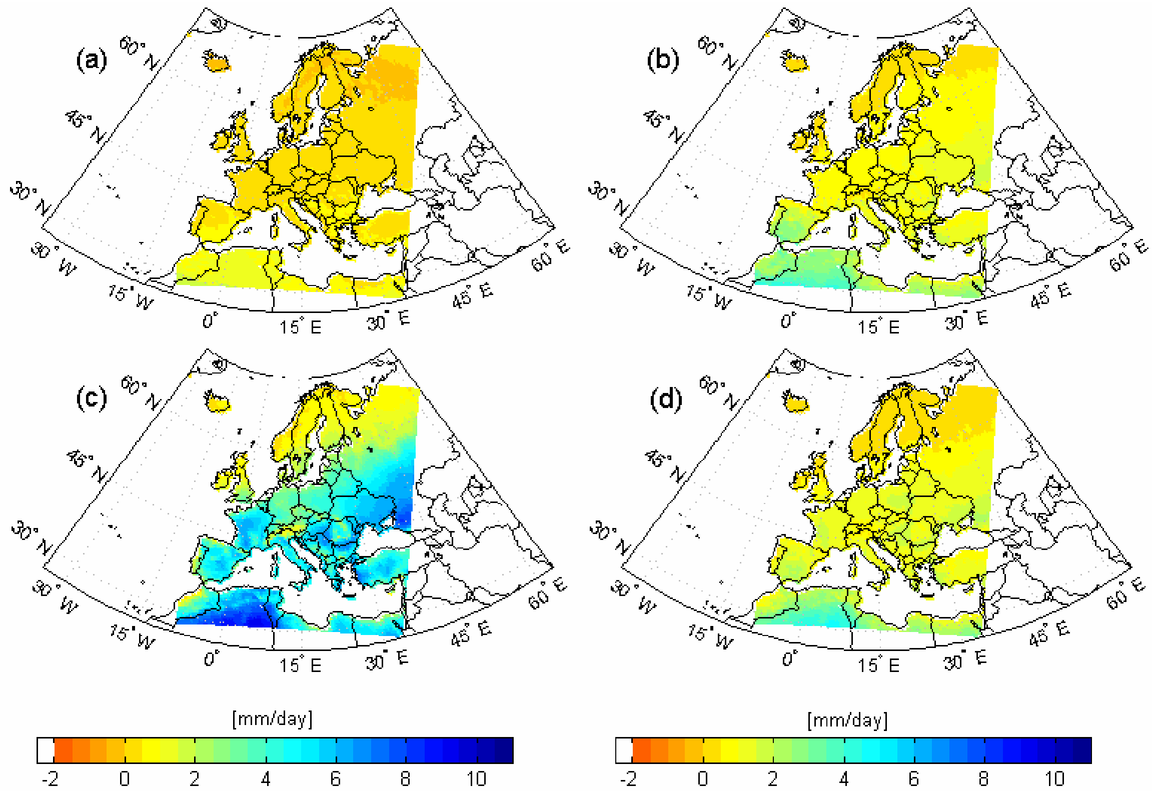

(a)
(b)
(c)
(d)
60° N
45° N
30° N
30° W
15° W
0°
15° E
30° E
45° E
60° E
[mm/day]
-2
0
2
4
6
8
10

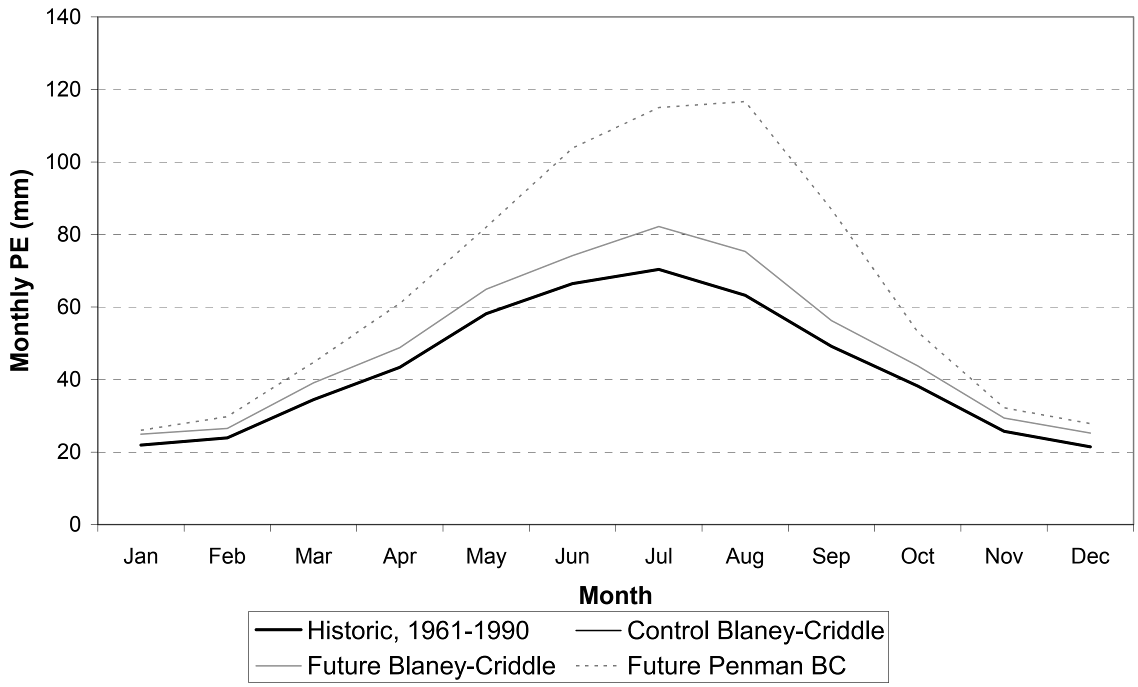

140
120
100
80
60
40
20
0
Monthly PE (mm)
Jan
Feb
Mar
Apr
May
Jun
Jul
Aug
Sep
Oct
Nov
Dec
Month
Historic, 1961-1990
Control Blaney-Criddle
Future Blaney-Criddle
Future Penman BC

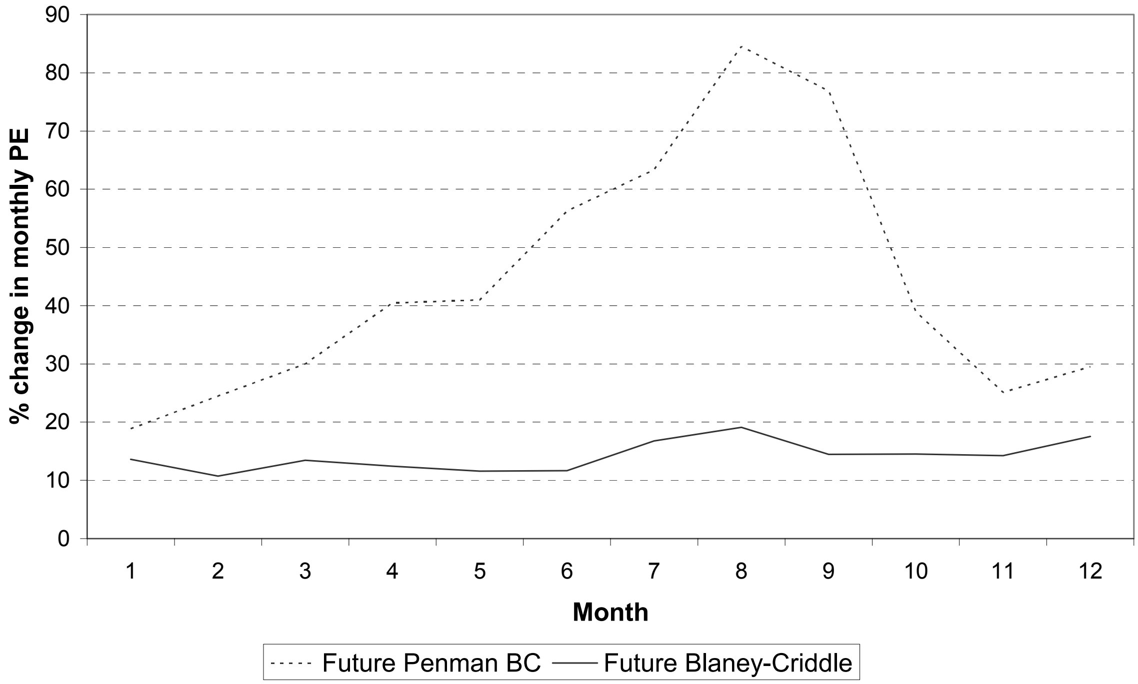

90
80
70
60
50
40
30
20
10
0
% change in monthly PE
1
2
3
4
5
6
7
8
9
10
11
12
Month
Future Penman BC
Future Blaney-Criddle

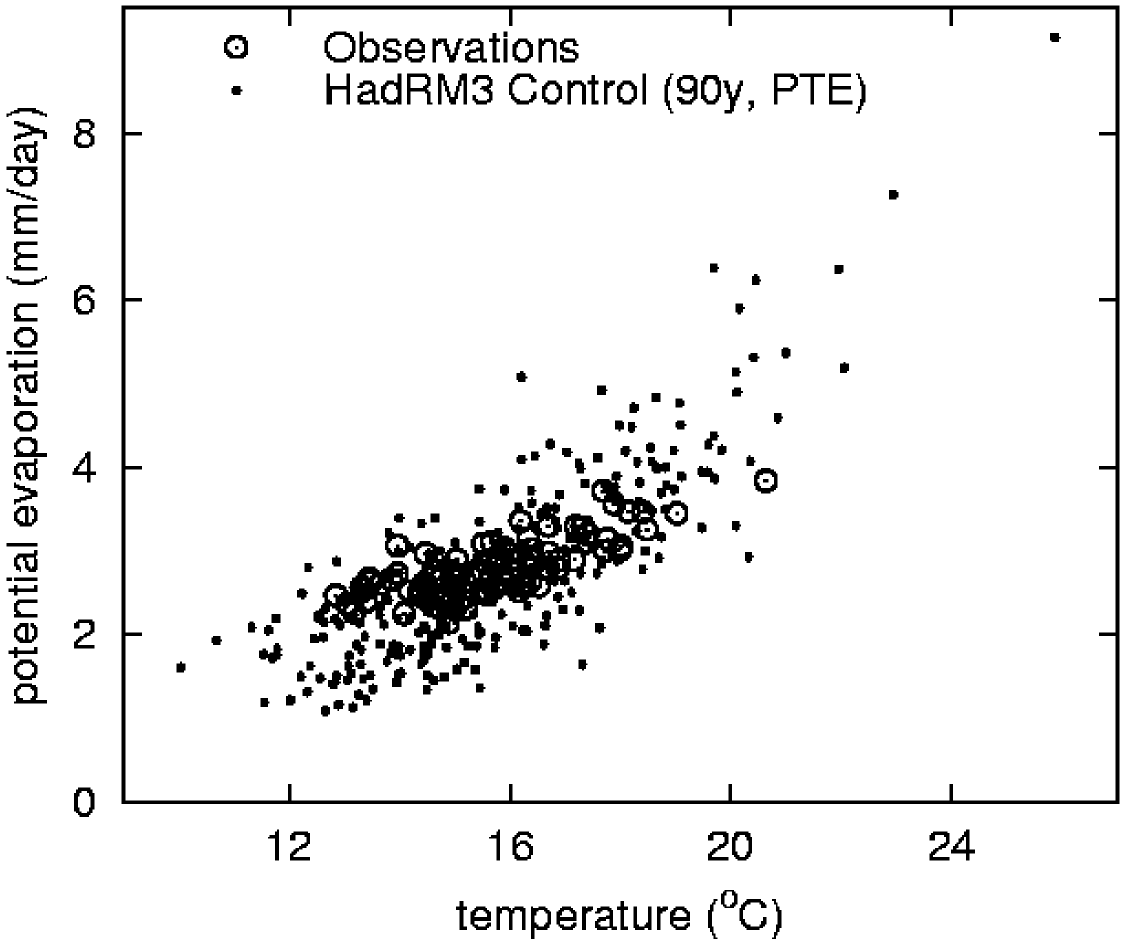
Observations
HadRM3 Control (90y, PTE)
potential evaporation (mm/day)
0
2
4
6
8
12
16
20
24
temperature (°C)

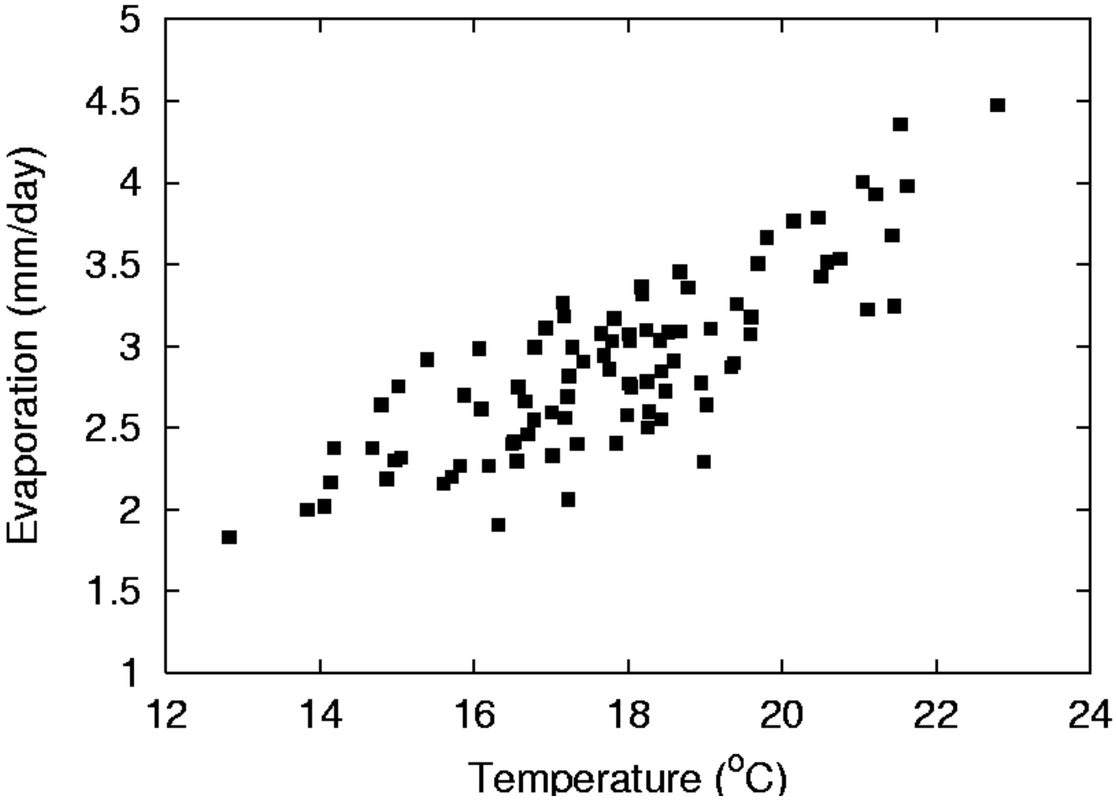

5
4.5
4
3.5
3
2.5
2
1.5
1
12
14
16
18
20
22
24
Evaporation (mm/day)
Temperature (^oC)

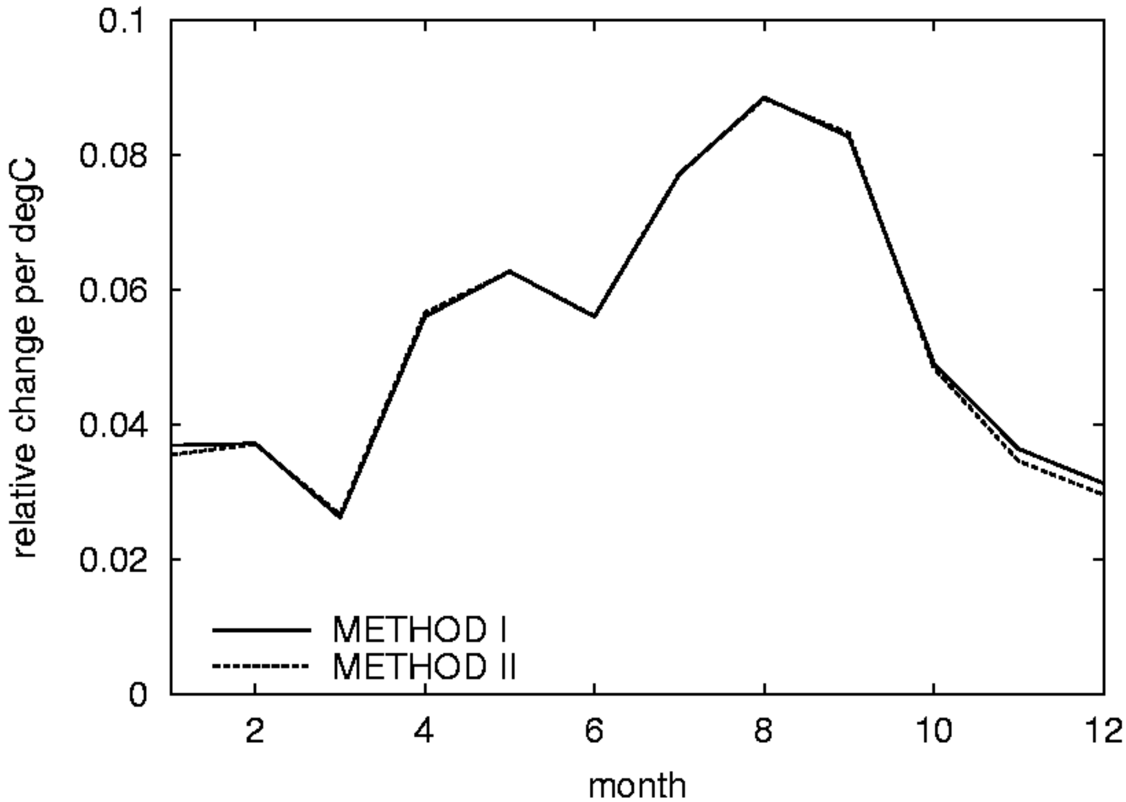
0.1
0.08
0.06
0.04
0.02
0
relative change per degC
2
4
6
8
10
12
month
METHOD I
METHOD II

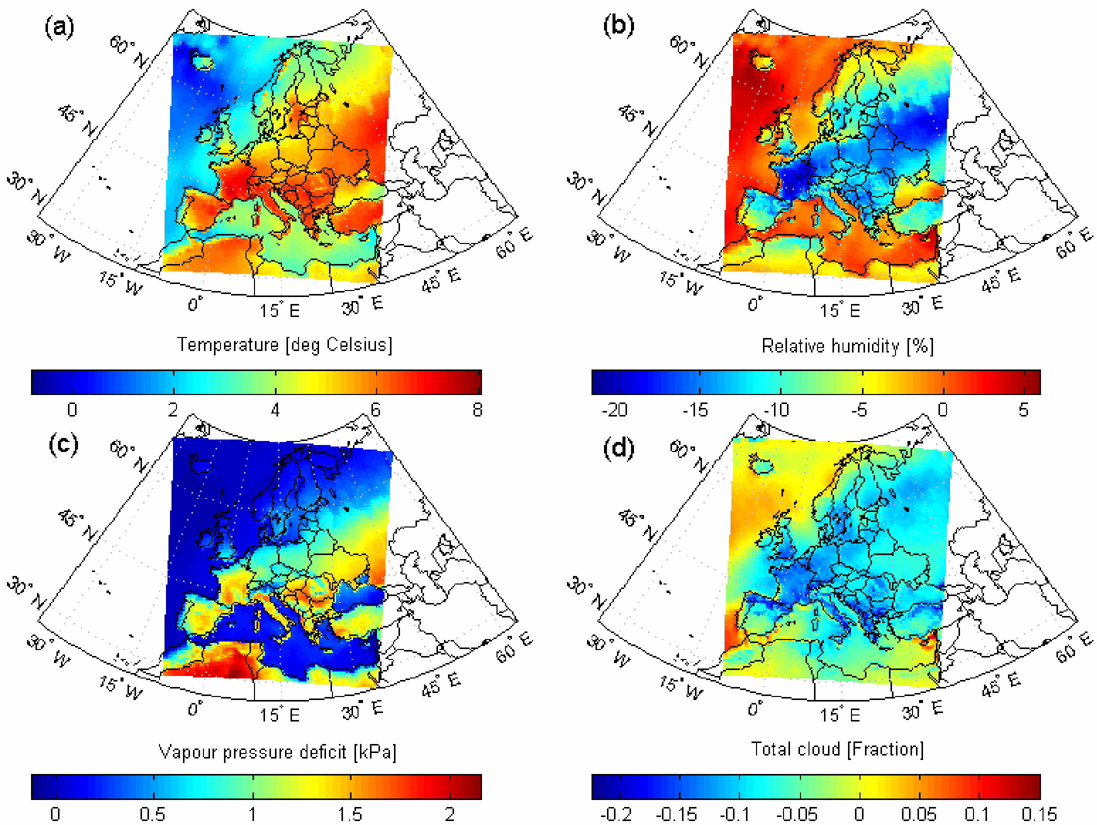
(a)
60° N
45° N
30° N
30° W
15° W
0°
15° E
30° E
45° E
60° E
Temperature [deg Celsius]
0
2
4
6
8
(b)
Relative humidity [%]
-20
-15
-10
-5
0
5
(c)
Vapour pressure deficit [kPa]
0
0.5
1
1.5
2
(d)
Total cloud [Fraction]
-0.2
-0.15
-0.1
-0.05
0
0.05
0.1
0.15